Datasheet for 600-401-106-0.1

Collagen Type IV Antibody

Overview

Description:	Anti-Collagen Type IV (RABBIT) Antibody - 600-401-106-0.1
Item No.:	600-401-106-0.1
Size:	100 µg
Applications:	Dot Blot, IHC, EM, IF, Multiplex, WB
Reactivity:	Human, Bovine
Host Species:	Rabbit

Product Details

Background:	Rockland produces highly active antibodies and conjugates to collagens. Collagens are highly conserved throughout evolution and are characterized by an uninterrupted ''Glycine-X-Y'' triplet repeat that is a necessary part of the triple helical structure. For these reasons, it is often extremely difficult to generate antibodies with specificities to collagens. The development of 'type' specific antibodies is dependent on NON-DENATURED three-dimensional epitopes. Rockland extensively purifies collagens for immunization from human and bovine placenta and cartilage by limited pepsin digestion and selective salt precipitation. This preparation results in a native conformation of the protein. Antibodies are isolated from rabbit antiserum and are extensively cross-adsorbed by immunoaffinity purification to produce 'type' specific antibodies. Greatly diminished reactivity and selectivity of these antibodies will result if denaturing and reducing conditions are used for SDS-PAGE and immunoblotting.
Synonyms:	rabbit anti-Collagen Type IV antibody, Arresten antibody, Canstatin antibody, Collagen Of Basement Membrane Alpha 1 Chain antibody, Collagen alpha-1 (IV) chain, COL4A1
Host Species:	Rabbit
Clonality:	Polyclonal
Format:	IgG

Target Details

Gene Name:	COL4A1-COL4A6
Reactivity:	Human, Bovine

Immunogen Type:	Native Protein
Immunogen:	Collagen Type IV from human and bovine placenta
Purity/Specificity:	Anti-Collagen Type IV has been prepared by immunoaffinity chromatography using immobilized antigens followed by extensive cross-adsorption against other collagens, human serum proteins and non-collagen extracellular matrix proteins to remove any unwanted specificities. Some class-specific anti-collagens may be specific for three-dimensional epitopes which may result in diminished reactivity with denatured collagen or formalin-fixed, paraffin embedded tissues. This antibody reacts with most mammalian Type IV collagens and has negligible cross-reactivity with Type I, II, III, V or VI collagens. Non-specific cross-reaction of anti-collagen antibodies with other human serum proteins or non-collagen extracellular matrix proteins is negligible.
Relevant Links:	• Anti-Collagen IHC Protocol • UniProtKB - P08572 • UniProtKB - P29400 • UniProtKB - P53420 • UniProtKB - Q01955 • UniProtKB - Q14031 • NCBI - NP_001290039.1 • UniProtKB - P02462 • GeneID - 1282

Application Details

Tested Applications:	Dot Blot, IHC
Suggested Applications:	EM, IF, Multiplex, WB (Based on references)
Application Note:	Anti-Collagen Type IV has been tested by dot blot and IHC and is suitable for indirect trapping ELISA for quantitation of antigen in serum using a standard curve, immunoprecipitation, native (non-denaturing, non-dissociating) PAGE, immunohistochemistry, and western blotting for highly sensitive qualitative analysis.
Assay Dilutions:	All assays should be optimized by the user. Recommended dilutions (if any) may be listed below.
ELISA:	1:5,000 - 1:50,000
IF:	User Optimized
IHC:	1:50 - 1:200
IP:	1:100
WB:	1:1,000 - 1:10,000

Other:	collagen hybridizing peptide (CHP) Staining - User Optimized

Formulation

Physical State:	Liquid (sterile filtered)
Concentration:	1.18 mg/mL by UV absorbance at 280 nm
Buffer:	0.02 M Potassium Phosphate, 0.15 M Sodium Chloride, pH 7.2
Preservative:	0.01% (w/v) Sodium Azide
Stabilizer:	None

Shipping & Handling

Shipping Condition:	Wet Ice
Storage Condition:	Store vial at 4° C prior to opening. This product is stable at 4° C as an undiluted liquid. Dilute only prior to immediate use. For extended storage, mix with an equal volume of glycerol, aliquot contents and freeze at -20° C or below. Avoid cycles of freezing and thawing.
Expiration:	Expiration date is one (1) year from date of receipt.

Images

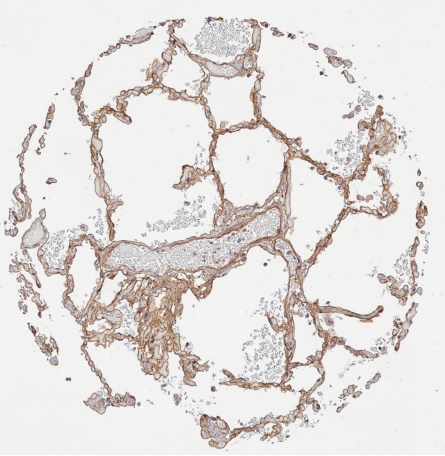

Immunohistochemistry
Immunohistochemistry results of Rabbit Anti-Collagen Type IV Antibody.
Tissue: human lung tissue.
Fixation: FFPE.
Antigen Retrieval: HIER using Tris-EDTA-citrate buffer pH 7.8 for 5 min.
Blocking: Peroxidase-Blocking Solution for 10 min.
Primary Antibody: Anti-Collagen Type IV (p/n 600-401-106-0.1) at 1:15 for 1 hr at 37 °C.
Secondary Antibody: Dako REAL EnVision Detection Kit, Polymer-HRP, Rabbit/Mouse.
Counterstain: Hematoxylin for 15 sec.
Substrate: DAB-Chromogen, Rabbit/Mouse.
Staining/Results: basement membranes and vessels.
Independently Validated by antibodies-online GmbH (p/n ABIN7565969/ ABIN5596835/ ABIN5596834) courtesy of MS Validated Antibodies.

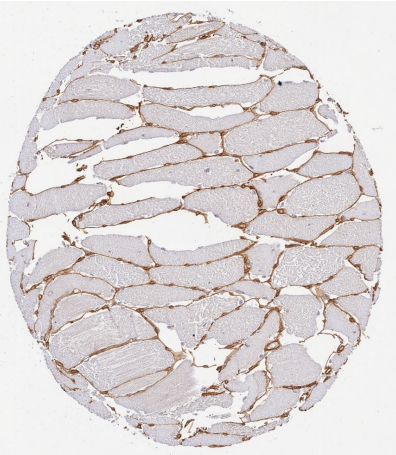

Immunohistochemistry
Immunohistochemistry results of Rabbit Anti-Collagen Type IV Antibody.
Tissue: human skeletal muscle cells.
Fixation: FFPE.
Antigen Retrieval: HIER using Tris-EDTA-citrate buffer pH 7.8 for 5 min.
Blocking: Peroxidase-Blocking Solution for 10 min.
Primary Antibody: Anti-Collagen Type IV (p/n 600-401-106-0.1) at 1:15 for 1 hr at 37 °C.
Secondary Antibody: Dako REAL EnVision Detection Kit, Polymer-HRP, Rabbit/Mouse.
Counterstain: Hematoxylin for 15 sec.
Substrate: DAB-Chromogen, Rabbit/Mouse.
Staining/Results: cells surrounded by collagen IV fibers.
Independently Validated by antibodies-online GmbH (p/n ABIN7565969/ ABIN5596835/ ABIN5596834) courtesy of MS Validated Antibodies.

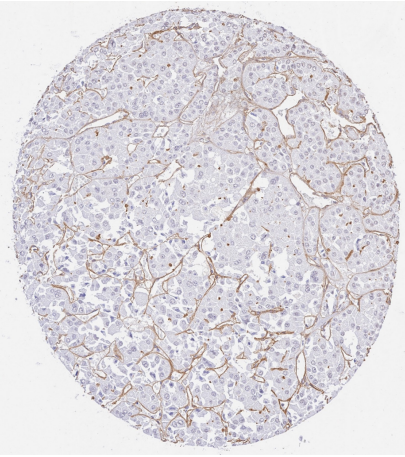

Immunohistochemistry
Immunohistochemistry results of Rabbit Anti-Collagen Type IV Antibody.
Tissue: human renal oncocytoma.
Fixation: FFPE.
Antigen Retrieval: HIER using Tris-EDTA-citrate buffer pH 7.8 for 5 min.
Blocking: Peroxidase-Blocking Solution for 10 min.
Primary Antibody: Anti-Collagen Type IV (p/n 600-401-106-0.1) at 1:15 for 1 hr at 37 °C.
Secondary Antibody: Dako REAL EnVision Detection Kit, Polymer-HRP, Rabbit/Mouse.
Counterstain: Hematoxylin for 15 sec.
Substrate: DAB-Chromogen, Rabbit/Mouse.
Staining/Results: dense collagen IV positive membranes surrounding tumor cell nests.
Independently Validated by antibodies-online GmbH (p/n ABIN7565969/ ABIN5596835/ ABIN5596834) courtesy of MS Validated Antibodies.

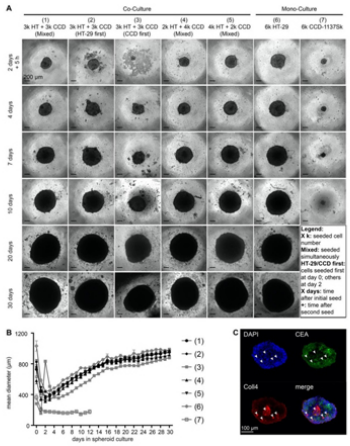

Immunofluorescence Microscopy

Growth of HT-29 spheroids is unaffected in the presence of CCD-1137Sk cells. Human HT-29 or CCD-1137Sk cells were seeded into ultra-low attachment plates to form spheroids, following different seeding orders (mixed, HT-29 first or CCD-1137Sk first) and cell numbers (ranging from 2000 to 6000 cells per type) as indicated. From 0 to 30 days in culture, brightfield images were taken to perform spheroid-size analysis based on the mean diameter (A–B). Additionally, co-culture spheroids with 250 HT-29 cells together with simultaneously seeded 500 CCD-1137Sk cells were fixed after four days and stained with DAPI as well as with anti-CEA and anti-Coll4 antibodies as markers for nuclei, HT-29 cells, and fibroblasts, respectively (C). (A) Representative brightfield images of HT-29 and CCD-1137Sk mono- and co-culture spheroids seeded in different ratios and orders, as depicted. (B) Graph shows a quantitative analysis of the mean diameters of mono- and co-culture spheroids at different time-points as indicated. Mean + SEM (n = 5–9 experiments). (C) Representative optical slice of DAPI (blue), anti-CEA (green), and anti-Coll4 signals (red). Arrowheads, exemplary clusters of Coll4-positive areas. Bottom right panel shows an overlay image of all three channels. Fig 4. PMID: 32823793

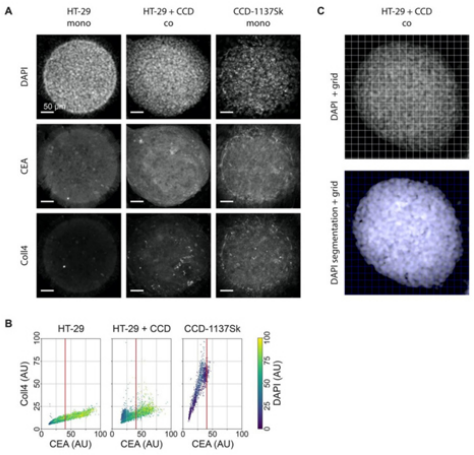

Immunofluorescence Microscopy
DAPI, CEA, and Coll4 staining jointly discriminate HT-29 and CCD-1137Sk cell populations in 3-D Dynarray co-cultures. A total of 4000 cells per chip cavity were seeded to yield either mono- or co-cultures of HT-29 and CCD-1137Sk cells. In case of co-cultures, 2000 HT-29 cells were co-seeded with 2000 CCD-1137Sk cells per well. After four days, chips were fixed, cleared, and stained with DAPI and antibodies against CEA and Coll4 as markers for nuclei, cancer cells, and fibroblasts, respectively. Subsequently, samples were imaged with 3-D confocal microscopy. (A) Representative sum-z projections. (B) Scatter plots showing the anti-Coll4 intensity distribution as a function of the anti-CEA intensity for HT-29 mono-cultures (left), HT-29 + CCD-1137Sk co-cultures (middle), and CCD-1137Sk mono-cultures (right). Each dot shows the average intensity of voxel cubes in a total of five Dynarray cavities. Red vertical line, CEA brightness range that contains 95% of all CCD-1137Sk voxel cubes in mono-culture. (C) Exemplary images showing the voxel-cube grid used for the quantification of the average fluorescence intensities. Upper panel, raw sum-z projection of DAPI signal; lower panel, sum-z projection upon nuclei segmentation and background subtraction. Fig 6. PMID: 32823793

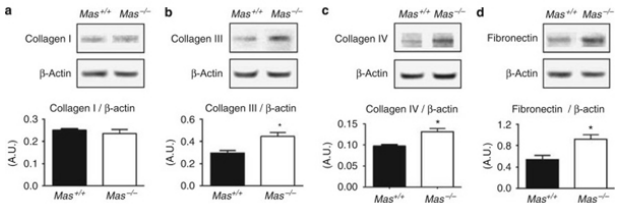

Western Blot
Immunoblotting of extracellular matrix (ECM) proteins in kidneys of Mas+/+ and Mas−/− animals. (a) Immunoblotting shows no difference of Collagen I (p/n 600-401-103) expression in Mas+/+ and Mas−/− mice kidneys. Significant increases in (b) Collagen III (p/n 600-401-105), (c) Collagen IV (p/n 600-401-106), and (d) fibronectin (p/n 600-401-117) expression were detected by comparing immunoblots of Mas−/− mouse kidneys with those of Mas+/+ controls. Each band represents one mouse kidney from either Mas+/+ or Mas−/− mice. Data are shown as the mean±s.e.m. *P<0.05. A.U. indicates arbitrary unit. Fig 5. PMID: 19262461

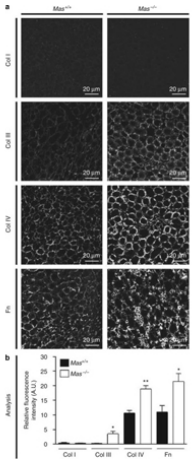

Immunofluorescence Microscopy
Immunofluorescence of extracellular matrix (ECM) proteins in the medulla of kidneys from Mas+/+ (left column) and Mas−/− (right column) mice. (a) Fluorescence (Cy3-labeled anti-rabbit IgG) reveals the immunolabeling of ECM proteins. Expression of type III collagen (Col III) (p/n 600-401 -105), type IV collagen (Col IV) (p/n 600-401-106), and fibronectin (Fn) (p/n 600-401-117) were increased in the medulla of Mas−/− compared with that of Mas+/+ mice, whereas the expression of type I collagen (Col I) (p/n 600-401-103) was unaltered. (b) Quantification of ECM proteins in the medulla of Mas+/+ and Mas−/− mice. Data are shown as mean±s.e.m. *P<0.05; **P<0.01. A.U. indicates arbitrary unit. Fig 3. PMID: 19262461

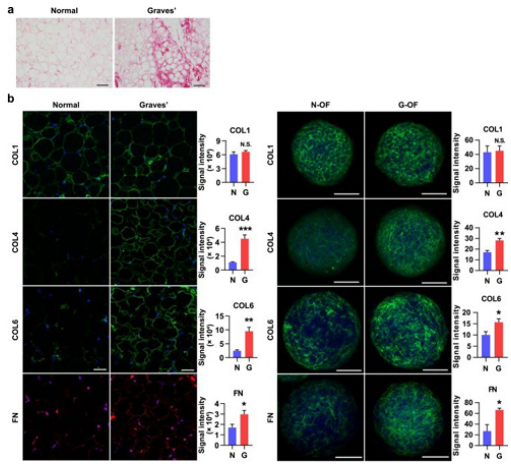

Immunofluorescence Microscopy
Unique ECM deposition in GO tissues and GO-derived OF organoids. (a) Representative Sirius red staining of periocular adipose tissues in control (normal) and GO (Graves). Scale bars, 100 µm. (b) Representative immunofluorescent staining of collagens (green) and FN (red or green) with DAPI (blue) in control and Graves orbital adipose tissues (left, n = 4 to 5) and 3D organoids reconstituted from hOFs isolated from respective tissues (right). Signal intensities were quantified per spheroid. n = 5 to 8 organoids. Scale bars, 50 µm (left) and 100 µm (right). G indicates G-OF; N indicates N-OF. *P < 0.05, unpaired Student t test (n = 4 in each group). Fig 2. PMID: 30388216

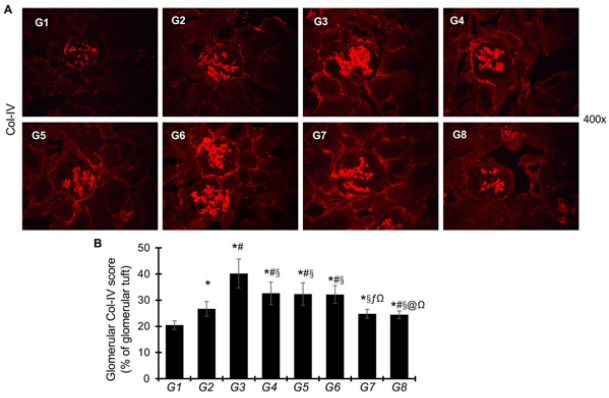

Immunofluorescence Microscopy
A: Representative photomicrographs of glomeruli with immunofluorescent staining for Col-IV derived from the following groups: G1: non-diabetic controls; G2: db/db-12 weeks; G3: db/db-18 weeks; G4: db/db+sGCa-Low dose; G5: db/db+sGCa-High dose; G6: db/db+ Empagliflozin (Empa); G7: db/db+Empa+sGCa-Low dose; G8: db/db+Empa+sGCa-High dose. Images are presented at 400x magnification. B: Graphic representation of glomerular Col-IV staining scores. Note: * vs G1, P<0.05; # vs G2, P<0.05; § vs G3, P<0.05; & G5 vs G4, P<0.05; ƒ, G7vs G4, P<0.05; @, G8 vs G5, P<0.05 and Ω G7 or G8 vs G6, P<0.05. Fig 4. PMID: 39907739

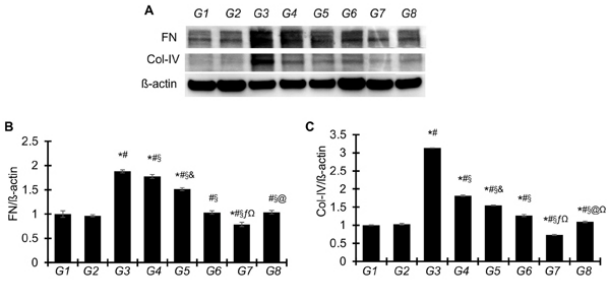

Western Blot

A: Representative Western blots demonstrating FN, Col IV, and ß-actin protein expression, isolated from renal cortex tissues derived from the following groups: G1: non-diabetic controls; G2: db/db-12 weeks; G3: db/db-18 weeks; G4: db/db+sGCa-Low dose; G5: db/db+sGCa-High dose; G6: db/db+ Empagliflozin (Empa); G7: db/db+Empa+sGCa-Low dose; G8: db/db+Empa+sGCa-High dose. B and C: Graphical representation summarizing the results of band density measurements for protein levels of FN (B) and Col-IV (C) in renal cortical tissues, corrected by the band density of ß-actin. The levels of FN or Col-IV/ß-actin in the non-diabetic control group were set as the unit. The levels of FN or Col-IV /ß-actin in other groups were express as fold changes over that of non-diabetic control group. Note: * vs G1, $P<0.05$; # vs G2, $P<0.05$; § vs G3, $P<0.05$; & G5 vs G4, $P<0.05$; ƒ, G7vs G4, $P<0.05$; @, G8 vs G5, $P<0.05$ and Ω G7 or G8 vs G6, $P<0.05$. Fig 4. PMID: 39907739

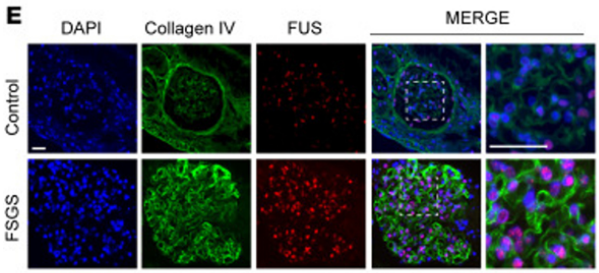

Immunofluorescence Microscopy

(E) Representative images of kidney and liver tissue samples from controls or individuals with FSGS or NASH costained with anti-FUS and anti–collagen IV antibodies. Scale bars: 25 µm. Fig 10. PMID: 38488009

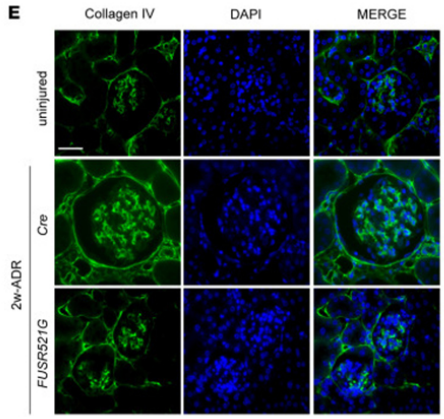

Immunofluorescence Microscopy
(E) Representative images of kidney sections from uninjured mice or mice treated with ADR for 2 weeks stained with anti–collagen IV antibody. Scale bar: 20 µm. Fig 5.
PMID: 38488009

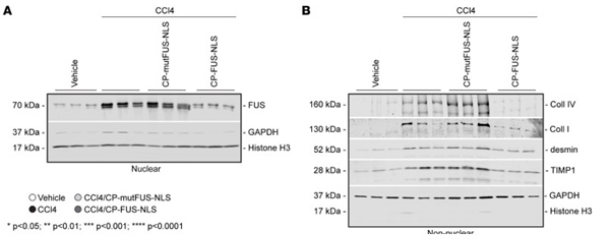

Western Blot
Nuclear fractions (50 µg/lane) of livers from uninjured (vehicle) mice and mice treated for 6 weeks with CCl4 alone or in combination with CP-mutFUS-NLS or CP-FUS-NLS peptide were analyzed by Western blot for FUS levels. Histone H3 and GAPDH were used to verify the purity of nuclear fractions. (B) Nonnuclear fractions (50 µg/lane) of livers from the mice described in A were analyzed by Western blot for levels of collagens I and IV, desmin, and TIMP1. Histone H3 and GAPDH were used to verify the purity of nonnuclear fractions. Fig 8. PMID: 38488009

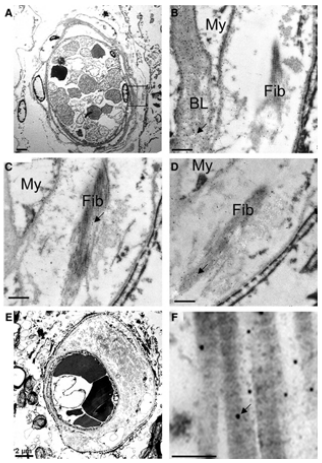

Immunofluorescence Microscopy
Immuno-electron microscopy of collagens I, III, and IV in small vessel disease (SVD). Transmission electron micrographs of small arteries in white matter from older persons with SVD. A–D, Semi-serial sections of a small arteriole, shown at low magnification in A and at higher magnification in B–D with immunogold labeling for collagen-IV (p/n 600-401-106) (B), collagen-I (p/n 600-401-103) (C), or collagen-III (p/n 600-401-105) (D). The region shown at higher magnification in B–D is marked in A (box). Arrows show examples of immunogold particles. In B, collagen-IV labeling shows numerous gold particles over the homogenous basal laminae (BL), behind the endothelium. Mural collagen fibrils (Fib) and myocytes (My) are unlabeled. C, Collagen-I, in contrast to collagen-IV, is mainly localized to the collagen fibrils. D, Collagen-III also labels the banded collagen fibrils. A few gold particles are found over the basal laminae. E and F, Another small artery with severe fibrosis. Low magnification view (E) shows heavy deposits of fibrillar collagens in the vessel wall. In higher magnification, these are heavily labeled for collagen-I (F). Scale bars: 2 µm (A and E), 0.5 µm (B–D), and 0.2 µm (F). Fig 3.
PMID: 36205142

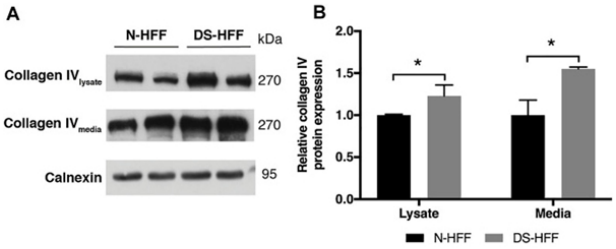

Western Blot
Trisomic samples show a significant increase of collagen IV protein in cell lysates and culture media. (A) Representative immunoblotting of collagen IV protein detected in cell lysates and media of three N-HFF and three DS-HFF samples. Calnexin was used as a loading control. (B) Densitometric analysis from three different experiments. Results are expressed as relative mean values ± SEM from three N-HFF and three DS-HFF samples. *p-value ≤ 0.05. Fig 5.
PMID: 35356434

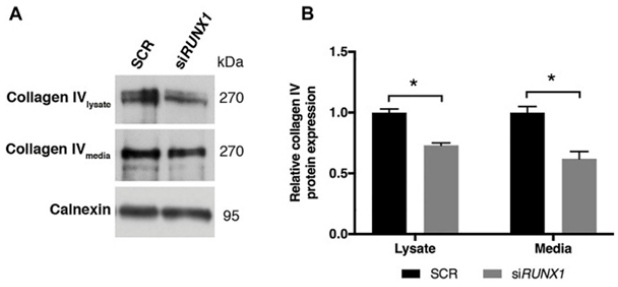

Western Blot
RUNX1 silencing leads to a significant decrease of collagen IV protein in media of silenced trisomic samples. (A) Representative immunoblotting of collagen IV protein detected in cell lysates and culture media of SCR and siRUNX1-treated DS-HFF samples. Calnexin was used as a loading control. (B) Densitometric analysis from two different experiments. In each experiment we used two out of the three DS-HFFs samples of Figure 5. Results are expressed as relative mean values ± SEM from two SCR and the two corresponding RUNX1-silenced DS-HFFs. *p-value ≤ 0.05. Fig 6. PMID: 35356434

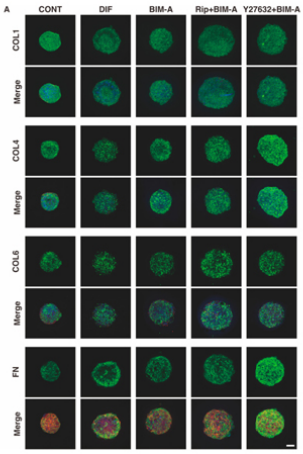

Immunofluorescence Microscopy
Representative confocal images showing the expression of ECMs in 3D 3T3-L1 spheroids under several sets of conditions. (A) On Day 7, the 3D cultures of spheroids of 3T3-L1 preadipocytes as the control (CONT), and their adipogenic differentiation in the absence (DIF) or presence of 100 nM bimatoprost free acid (BIM-A) and/or 10 µM ROCK-i (Rip or Y27632), were immunostained with specific antibodies of ECMs designated by the green color. Scale bar: 100 µm. Fig 9.
PMID: 36421103

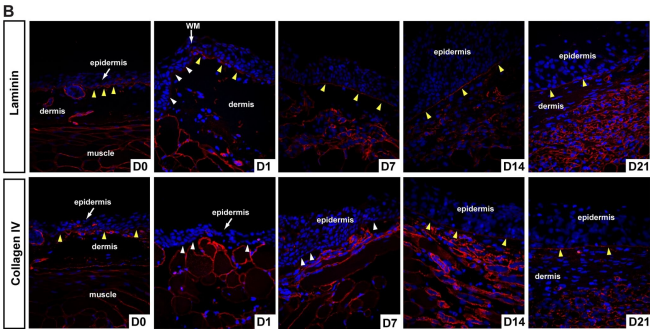

Immunohistochemistry

Lamina lucida and lamina densa regenerate before new ECM deposition.A) Histological examination of basement membrane (BM) regeneration in axolotls. The uninjured BM is visible as a thick blue-stained fibrous band (yellow arrows). An immature BM has begun to reform (yellow arrow D1) after re-epithelialization and is visible at the wound margin (WM) in contrast to the uninjured BM. The regenerated BM is visible at D47. Yellow arrows at D7 and D21 indicate reforming BM. B) Examination of lamina lucida (laminin) and lamina densa (collagen type IV) during basement membrane regeneration. The uninjured BM is positive for laminin and collagen type IV (yellow arrows) as are the basement membranes surrounding glands and muscle fibers. Following re-epithelialization the basal lamina of the epidermis is negative for laminin and collagen type IV (white arrows) and this is clearly evident at the wound margin (WM). Seven days post injury the BM stains strongly for laminin indicating reformation of the lamina lucida, while staining for collagen type IV is punctuated. The lamina densa is regenerated by D14 based on continuous collagen type IV staining and persists during dermal regeneration. Figure provided by CiteAb. Source: PLoS One, PMID: 22485136.

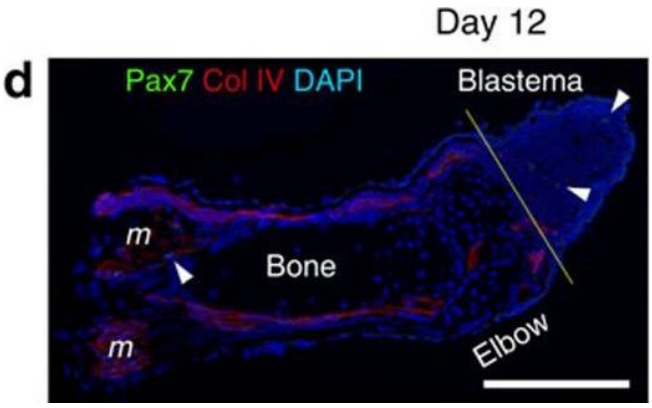

Immunohistochemistry

SMFC tracking in larval newt limb regeneration.(a) Larva (3 months old). It has four limbs, as well as the gills and tail fin. Scale bar, 4 mm. (b) Monitoring of SMFCs (mCherry+) during limb regeneration (n=6). mCherry was not detected in the regenerating part of the limb until ⍰30 days when the amputated limb had almost been recovered (see Supplementary Movie 1). Arrowheads: flexor muscle for digits (see Fig. 2). Scale bar, 1 mm. (c) Sections of regenerating limbs (n=3 for each stage). SMFC-derived mCherry+ cells were not observed in the blastema. Lines: amputation site. m: muscle. Scale bar, 100 µm. (d–f) Pax7 immunolabelling of regenerating limbs on day 12 (n=3) and (g) day 15 (n=3) after amputation. (d) On day 12, a few Pax7+ nuclei (arrowheads) were detected in blastema cells and in satellite cells along the muscle fibres. Col IV, collagen type IV immunoreactivity. DAPI (4,6-diamidino-2-phenylindole), nuclei. Scale bar, 300 µm. The Pax7+ nuclei pointed by arrowheads were enlarged in e and f, respectively. Scale bars, 100 µm. (g) On day 15 when the regenerating part of the limb grew more distally, the number of Pax7+ nuclei (arrowheads) in the blastema was dramatically increased. Scale bar, 100 µm. (h) Summary. In larval newts, MPCs, potentially satellite cells, were recruited for new muscle during limb regeneration, whereas SMFCs were not. Figure provided by CiteAb. Source: Nat Commun, PMID: 27026263.

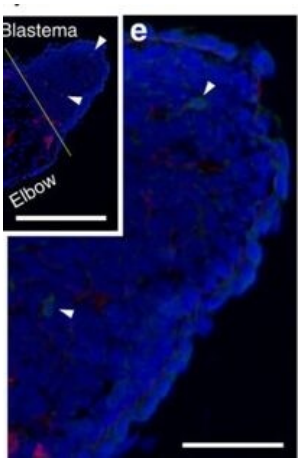

Immunohistochemistry

SMFC tracking in larval newt limb regeneration.(a) Larva (3 months old). It has four limbs, as well as the gills and tail fin. Scale bar, 4 mm. (b) Monitoring of SMFCs (mCherry+) during limb regeneration (n=6). mCherry was not detected in the regenerating part of the limb until ⍰30 days when the amputated limb had almost been recovered (see Supplementary Movie 1). Arrowheads: flexor muscle for digits (see Fig. 2). Scale bar, 1 mm. (c) Sections of regenerating limbs (n=3 for each stage). SMFC-derived mCherry+ cells were not observed in the blastema. Lines: amputation site. m: muscle. Scale bar, 100 µm. (d–f) Pax7 immunolabelling of regenerating limbs on day 12 (n=3) and (g) day 15 (n=3) after amputation. (d) On day 12, a few Pax7+ nuclei (arrowheads) were detected in blastema cells and in satellite cells along the muscle fibres. Col IV, collagen type IV immunoreactivity. DAPI (4,6-diamidino-2-phenylindole), nuclei. Scale bar, 300 µm. The Pax7+ nuclei pointed by arrowheads were enlarged in e and f, respectively. Scale bars, 100 µm. (g) On day 15 when the regenerating part of the limb grew more distally, the number of Pax7+ nuclei (arrowheads) in the blastema was dramatically increased. Scale bar, 100 µm. (h) Summary. In larval newts, MPCs, potentially satellite cells, were recruited for new muscle during limb regeneration, whereas SMFCs were not. Figure provided by CiteAb. Source: Nat Commun, PMID: 27026263.

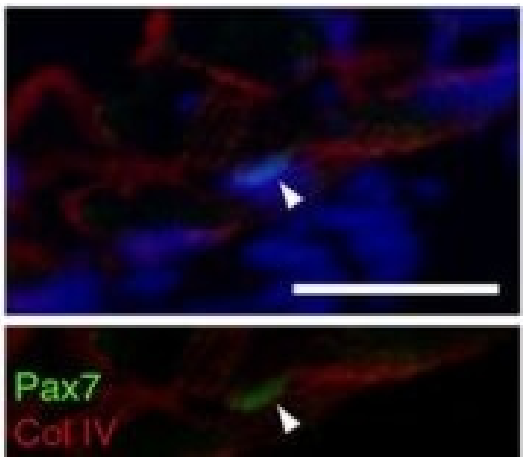

Immunohistochemistry
SMFC tracking in larval newt limb regeneration.(a) Larva (3 months old). It has four limbs, as well as the gills and tail fin. Scale bar, 4 mm. (b) Monitoring of SMFCs (mCherry+) during limb regeneration (n=6). mCherry was not detected in the regenerating part of the limb until ⍰30 days when the amputated limb had almost been recovered (see Supplementary Movie 1). Arrowheads: flexor muscle for digits (see Fig. 2). Scale bar, 1 mm. (c) Sections of regenerating limbs (n=3 for each stage). SMFC-derived mCherry+ cells were not observed in the blastema. Lines: amputation site. m: muscle. Scale bar, 100 µm. (d–f) Pax7 immunolabelling of regenerating limbs on day 12 (n=3) and (g) day 15 (n=3) after amputation. (d) On day 12, a few Pax7+ nuclei (arrowheads) were detected in blastema cells and in satellite cells along the muscle fibres. Col IV, collagen type IV immunoreactivity. DAPI (4,6-diamidino-2-phenylindole), nuclei. Scale bar, 300 µm. The Pax7+ nuclei pointed by arrowheads were enlarged in e and f, respectively. Scale bars, 100 µm. (g) On day 15 when the regenerating part of the limb grew more distally, the number of Pax7+ nuclei (arrowheads) in the blastema was dramatically increased. Scale bar, 100 µm. (h) Summary. In larval newts, MPCs, potentially satellite cells, were recruited for new muscle during limb regeneration, whereas SMFCs were not. Figure provided by CiteAb. Source: Nat Commun, PMID: 27026263.

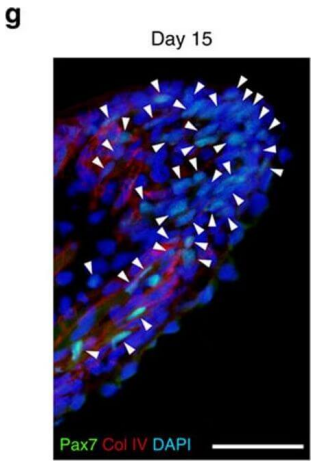

Immunohistochemistry

SMFC tracking in larval newt limb regeneration.(a) Larva (3 months old). It has four limbs, as well as the gills and tail fin. Scale bar, 4 mm. (b) Monitoring of SMFCs (mCherry+) during limb regeneration (n=6). mCherry was not detected in the regenerating part of the limb until ⍰30 days when the amputated limb had almost been recovered (see Supplementary Movie 1). Arrowheads: flexor muscle for digits (see Fig. 2). Scale bar, 1 mm. (c) Sections of regenerating limbs (n=3 for each stage). SMFC-derived mCherry+ cells were not observed in the blastema. Lines: amputation site. m: muscle. Scale bar, 100 µm. (d–f) Pax7 immunolabelling of regenerating limbs on day 12 (n=3) and (g) day 15 (n=3) after amputation. (d) On day 12, a few Pax7+ nuclei (arrowheads) were detected in blastema cells and in satellite cells along the muscle fibres. Col IV, collagen type IV immunoreactivity. DAPI (4,6-diamidino-2-phenylindole), nuclei. Scale bar, 300 µm. The Pax7+ nuclei pointed by arrowheads were enlarged in e and f, respectively. Scale bars, 100 µm. (g) On day 15 when the regenerating part of the limb grew more distally, the number of Pax7+ nuclei (arrowheads) in the blastema was dramatically increased. Scale bar, 100 µm. (h) Summary. In larval newts, MPCs, potentially satellite cells, were recruited for new muscle during limb regeneration, whereas SMFCs were not. Figure provided by CiteAb. Source: Nat Commun, PMID: 27026263.

Immunohistochemistry

SMFC tracking in metamorphosed newt limb regeneration. (a) Juvenile (16 months old). Scale bar, 15 mm. (b) Limb regeneration. Scale bar, 5 mm. (c–e) Tracking of SMFCs (mCherry+) (n=2). This animal was a mosaic expressing EGFP in muscle only. mCherry+ fibres in the forearm were ?25% of total EGFP+ fibres. (c) On day 36 after amputation, fragments of muscle fibres (arrows) were observed in distal regions adjacent to the blastema. Scale bar, 100 µm. (d) mCherry+ mononucleated cells (red arrowheads; enlarged in right-hand panels) and EGFP+ cells (green arrowheads) were observed in the blastema. Epi, epidermis. To-pro-3: nuclei. Scale bars, 50 µm (left), 10 µm (right-hand panels). (e) In the same limb, at day 96 after the second amputation in the upper arm (line), mCherry (arrows) and EGFP were observed only in muscle fibres. Scale bars, 1 mm (upper panel), 500 µm (lower panels). (f–i) Pax7 immunolabelling of a regenerating limb on day 26 after amputation (n=4). Pax7 immunoreactivity was not detected in the blastema. (f) Translucent image. Line: amputation site. (g) Merged fluorescence image. Col IV, collagen type IV immunoreactivity. To-pro-3: nuclei. Scale bar, 1 mm. (h) Enlargement of a region in the blastema and (i) a region proximal to the amputation site, enclosed by boxes in g. Scale bars, 250 µm. Arrowheads in (i) Pax7+ nuclei. An example satellite cell (box) is enlarged in the right-hand panels (upper: Col VI/To-pro-3; lower: Col IV/Pax7). Scale bar, 50 µm. (j) Summary. In metamorphosed newts, SMFCs were recruited for new muscle during limb regeneration, whereas MPCs such as satellite cells were not. Figure provided by CiteAb. Source: Nat Commun, PMID: 27026263.

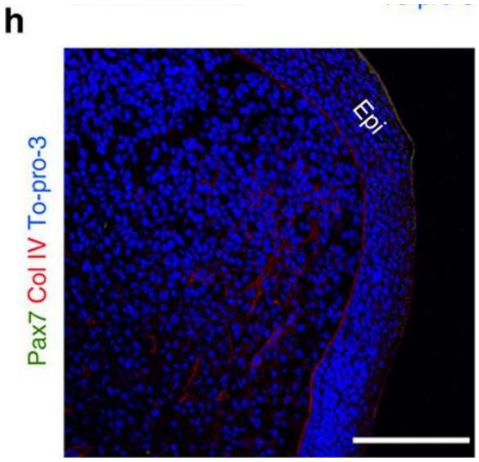

Immunohistochemistry

SMFC tracking in metamorphosed newt limb regeneration. (a) Juvenile (16 months old). Scale bar, 15 mm. (b) Limb regeneration. Scale bar, 5 mm. (c–e) Tracking of SMFCs (mCherry+) (n=2). This animal was a mosaic expressing EGFP in muscle only. mCherry+ fibres in the forearm were ≈25% of total EGFP+ fibres. (c) On day 36 after amputation, fragments of muscle fibres (arrows) were observed in distal regions adjacent to the blastema. Scale bar, 100 µm. (d) mCherry+ mononucleated cells (red arrowheads; enlarged in right-hand panels) and EGFP+ cells (green arrowheads) were observed in the blastema. Epi, epidermis. To-pro-3: nuclei. Scale bars, 50 µm (left), 10 µm (right-hand panels). (e) In the same limb, at day 96 after the second amputation in the upper arm (line), mCherry (arrows) and EGFP were observed only in muscle fibres. Scale bars, 1 mm (upper panel), 500 µm (lower panels). (f–i) Pax7 immunolabelling of a regenerating limb on day 26 after amputation (n=4). Pax7 immunoreactivity was not detected in the blastema. (f) Translucent image. Line: amputation site. (g) Merged fluorescence image. Col IV, collagen type IV immunoreactivity. To-pro-3: nuclei. Scale bar, 1 mm. (h) Enlargement of a region in the blastema and (i) a region proximal to the amputation site, enclosed by boxes in g. Scale bars, 250 µm. Arrowheads in (i) Pax7+ nuclei. An example satellite cell (box) is enlarged in the right-hand panels (upper: Col VI/To-pro-3; lower: Col IV/Pax7). Scale bar, 50 µm. (j) Summary. In metamorphosed newts, SMFCs were recruited for new muscle during limb regeneration, whereas MPCs such as satellite cells were not. Figure provided by CiteAb. Source: Nat Commun, PMID: 27026263.

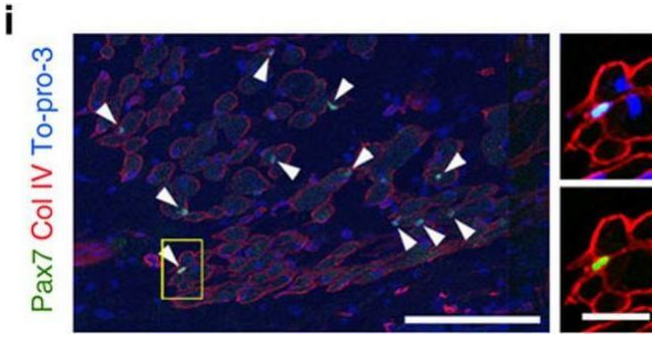

Immunohistochemistry
SMFC tracking in metamorphosed newt limb regeneration. (a) Juvenile (16 months old). Scale bar, 15 mm. (b) Limb regeneration. Scale bar, 5 mm. (c–e) Tracking of SMFCs (mCherry+) (n=2). This animal was a mosaic expressing EGFP in muscle only. mCherry+ fibres in the forearm were ⍰25% of total EGFP+ fibres. (c) On day 36 after amputation, fragments of muscle fibres (arrows) were observed in distal regions adjacent to the blastema. Scale bar, 100 µm. (d) mCherry+ mononucleated cells (red arrowheads; enlarged in right-hand panels) and EGFP+ cells (green arrowheads) were observed in the blastema. Epi, epidermis. To-pro-3: nuclei. Scale bars, 50 µm (left), 10 µm (right-hand panels). (e) In the same limb, at day 96 after the second amputation in the upper arm (line), mCherry (arrows) and EGFP were observed only in muscle fibres. Scale bars, 1 mm (upper panel), 500 µm (lower panels). (f–i) Pax7 immunolabelling of a regenerating limb on day 26 after amputation (n=4). Pax7 immunoreactivity was not detected in the blastema. (f) Translucent image. Line: amputation site. (g) Merged fluorescence image. Col IV, collagen type IV immunoreactivity. To-pro-3: nuclei. Scale bar, 1 mm. (h) Enlargement of a region in the blastema and (i) a region proximal to the amputation site, enclosed by boxes in g. Scale bars, 250 µm. Arrowheads in (i) Pax7+ nuclei. An example satellite cell (box) is enlarged in the right-hand panels (upper: Col VI/To-pro-3; lower: Col IV/Pax7). Scale bar, 50 µm. (j) Summary. In metamorphosed newts, SMFCs were recruited for new muscle during limb regeneration, whereas MPCs such as satellite cells were not. Figure provided by CiteAb. Source: Nat Commun, PMID: 27026263.

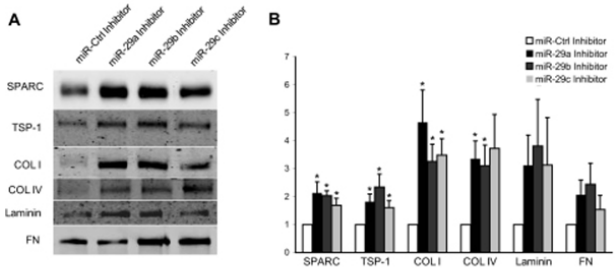

Western Blot
Inhibition of the miR-29 family induces ECM synthesis. (A) Representative immunoblot and (B) densitometric analyses of ECM proteins from conditioned media of TM cells transfected with miR control, miR-29a, miR-29b, or miR-29c inhibitors. All data are expressed as the mean ± SEM (*P < 0.05 vs. corresponding miR-Ctrl Inhibitor group; n = 5, where n refers to the number of independent experiments performed using n different primary human TM cell strains). Fig 5. PMID: 21330653

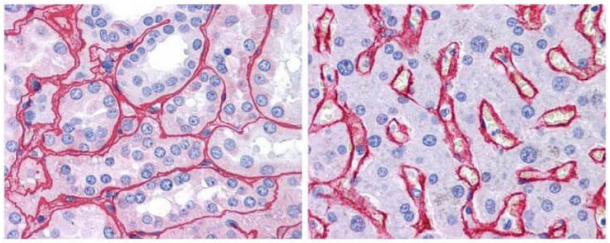

Immunohistochemistry
Rockland anti collagen IV antibody (600-401-106 Lot 25440, 1:400, 45 min RT) showed strong staining in FFPE sections of human kidney (Left) with strong red staining observed in glomeruli; and liver (Right) with strong staining in sinusoids. Staining for both tissues was consistent with a basement membrane distribution. Slides were steamed in 0.01 M sodium citrate buffer, pH 6.0 at 99-100°C - 20 minutes for antigen retrieval. Images provided courtesy of LifeSpan Biosciences, Seattle, WA

References

- Sharma N et al. A novel soluble guanylate cyclase activator, avenciguat, in combination with empagliflozin, protects against renal and hepatic injury in diabetic db/db mice. *Am J Physiol Endocrinol Metab.* (2025)
- Chiusa M et al. Cytoplasmic retention of the DNA/RNA-binding protein FUS ameliorates organ fibrosis in mice. *J Clin Invest.* (2024)
- Tsugeno Y et al. All Trans-Retinoic Acids Facilitate the Remodeling of 2D and 3D Cultured Human Conjunctival Fibroblasts. *Bioengineering (Basel).* (2022)
- Yu Z et al. The latent dedifferentiation capacity of newt limb muscles is unleashed by a combination of metamorphosis and body growth. *Scientific Reports* (2022)
- Ida, Y et al. ROCK 1 and 2 affect the spatial architecture of 3D spheroids derived from human corneal stromal fibroblasts in different manners. *Scientific Reports* (2022)
- Suzuki, S et al. Comparison of the Drug-Induced Efficacies between Omidenepag Isopropyl, an EP2 Agonist and PGF2α toward TGF-β2-Modulated Human Trabecular Meshwork (HTM) Cells. *Journal of Clinical Medicine* (2022)
- Sasaki K et al. Macrophage interferon regulatory factor 4 deletion ameliorates aristolochic acid nephropathy via reduced migration and increased apoptosis. *JCI Insight* (2022)
- Hu C et al. Multiomic identification of factors associated with progression to cystic kidney disease in mice with nephron Ift88 disruption. *Am J Physiol Renal Physiol.* (2022)
- Ida Y et al. Addition of ROCK Inhibitors Alleviates Prostaglandin-Induced Inhibition of Adipogenesis in 3T3L-1 Spheroids. *Bioengineering (Basel).* (2022)
- Kumar AA et al. Vascular Collagen Type-IV in Hypertension and Cerebral Small Vessel Disease. *Stroke.* (2022)
- Mollo N et al. Overexpression of the Hsa21 Transcription Factor RUNX1 Modulates the Extracellular Matrix in Trisomy 21 Cells. *Front Genet.* (2022)
- View More ...

Disclaimer

This product is for research use only and is not intended for therapeutic or diagnostic applications. Please contact a technical service representative for more information. All products of animal origin manufactured by Rockland Immunochemicals are derived from starting materials of North American origin. Collection was performed in United States Department of Agriculture (USDA) inspected facilities and all materials have been inspected and certified to be free of disease and suitable for exportation. All properties listed are typical characteristics and are not specifications. All suggestions and data are offered in good faith but without guarantee as conditions and methods of use of our products are beyond our control. All claims must be made within 30 days following the date of delivery. The prospective user must determine the suitability of our materials before adopting them on a commercial scale. Suggested uses of our products are not recommendations to use our products in violation of any patent or as a license under any patent of Rockland Immunochemicals, Inc. If you require a commercial license to use this material and do not have one, then return this material, unopened to: Rockland Inc., P.O. BOX 5199, Limerick, Pennsylvania, USA.